Supporting Information

Prentice-Mott et al. 10.1073/pnas.1317441110

Timing of Retraction Event Correlates with Cell Length

We observed that the length of time over which the cell was extending two pseudopods before retraction increased with increasing cell length (Fig. S4A). We eliminated the notion that these cells moved slower by measuring velocities in wider and narrower channels and seeing no difference in cell motility rates (Fig. S4C). As shown in Fig. S4B, longer cells extended longer pseudopods, but because there is no obvious difference in velocities between long and short cells, the longer cells must have taken a longer time to decide. Two appealing models could explain this observed relationship. First, every cell might extend a specific fraction into the bifurcations before retracting one leading edge. Thus, the cell will not retract one leading edge until the distance between the bifurcation and the back of the cell is a certain fraction of the cell length. Second, the absolute distance of the back of the cell from the bifurcation determines when the cell retracts one leading edge. Fig. S4D shows the fractional back distance vs. the cell length. A linear regression to this data (not shown) gives a negative slope, which is significantly different from 0. This suggests that the fractional back distance is not an invariant with respect to cell length. If, on the contrary, the absolute distance of the back from the bifurcation is invariant with respect to cell length, the data would fit a hyperbolic curve. Fitting the data with the hyperbolic function $Y = A/X$ gives a value for A of 7.642 ($r^2 = 0.991$). This would imply that the cell does not decide which direction to migrate until the back of the cell is ~7.5 μm from the center of the bifurcation.

One potential mechanism by which the absolute back distance could regulate the timing of the directional decision is through cytoskeletal tension. Cortical actomyosin as well as activated myosin are both polarized to the back of the cell during migration. This would suggest that the uropod of the cell is quite stiff. As this stiff structure approaches the bifurcation, it could experience increased tension as a result of being pulled around the corners of the bifurcation. This increase in tension may elicit a signaling event from the back of the cell to the front—a diffusible signal or via membrane tension—to signal the retraction of the shorter pseudopod. Further studies would be required to identify the activating step for pseudopod retraction, but the analysis here favors a back-generated signal.
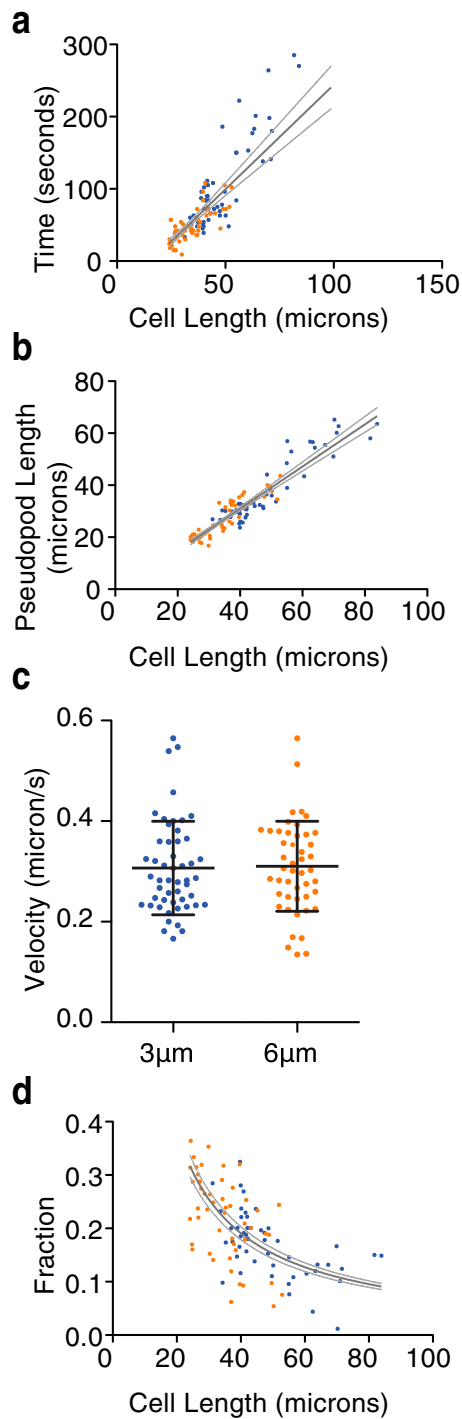
Fig. S1. Asymmetric directional bias requires extension of two pseudopods. (A and B) Time course montages of a cell extending two pseudopods ("two") (A) and only a single pseudopod ("one") (B). (Scale bar, 10 μm.) (C) Directional decision statistics for cells extending only a single pseudopod in the various geometries and in the presence or absence of chemokine. Statistics are shown for 1× and 4× length and resistance ratios. N represents the number of cells observed. (D) Bar graph indicating the percentage of total cells which extended only a single pseudopod. Conditions not shown had fewer than 10 cells extending only a single pseudopod.

Fig. S2. Spatiotemporal image correlation spectroscopy (STICS) data analysis. (*A*) Representative plot of the correlation coefficient as a function of temporal and spatial lag. Dashed line shows position of center of Gaussian peak found by fit. (*B*) Same plot as in *A*, but magnified to show movement of Gaussian peak. (*C*) A 3D plot of full spatiotemporal correlation function. (*D*) Amplitude of the Gaussian fit of the correlation as a function of the time lag. Solid line is a nonlinear least-squares fit of the decay according to the function described previously (1). (*E*) Scatter plot of measured fluid velocity vs. cell velocity when using entire channel, rather than only the region excluding the cell, for STICS algorithm. Nonlinear regression gave a slope of 1.01 ± 0.09 and an intercept of −0.01 ± 0.02.

1. Hebert B, Costantino S, Wiseman PW (2005) Spatiotemporal image correlation spectroscopy (STICS) theory, verification, and application to protein velocity mapping in living CHO cells. *Biophys J* 88(5):3601–3614.

Fig. S3. Initial asymmetries do not correlate strongly with cellular directional decision. (*A–D*) Scatter dot plots of the normalized extension rate (*A* and *C*) and 3xPH-Akt-GFP (PH-Akt) polarization (*B* and *D*) as the cell entered the bifurcation for 4× (*A* and *B*) and 1× (*C* and *D*) resistance ratios. For all plots, the distribution for cells in both channel width geometries is shown in black. The distribution for cells that migrate toward the low-resistance/right side is shown in green, grouped by bifurcation channel width. The distribution for cells that migrated toward the high-resistance/left side is shown in red, grouped by bifurcation channel width.

Fig. S4. Timing of the cell decision is influenced by cell back-bifurcation distance. (*A*) Scatter plot of time between the bifurcation entry and retraction times vs. the cell length. Solid line is a linear regression of the data, and the dashed lines are the 95% confidence bands for the fitting. Orange points indicate cells in wide channels, and blue points indicate cells in narrow channels. (*B*) Scatter plot of the total length of both pseudopods extended vs. cell length. Lines show a linear regression (solid line) and the 95% confidence bands (dashed line). Orange points indicate cells in wide channels, and blue points indicate cells in narrow channels. (*C*) Uropod velocities from cells migrating in wide and narrow channels. (*D*) Scatter plot of the fractional back distance (relative to cell length) vs. cell length. Orange points indicate cells in wide channels, and blue points indicate cells in narrow channels. Hyperbolic fit to data is shown.
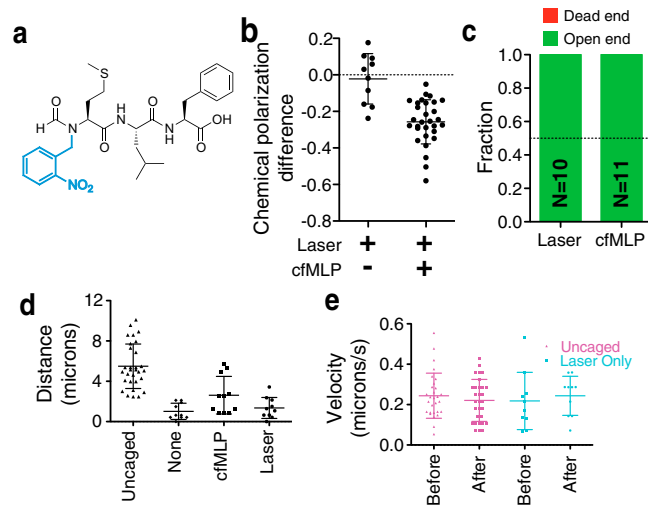
Fig. S5. Characterization of caged *N*-formyl-methionyl-leucyl-phenylalanine (cfMLP). (*A*) Chemical structure of caged compound. Nitro-benzyl group highlighted in cyan. (*B*) Scatter dot plot showing the maximum change in polarization of cells directly before and within 21 s following laser activation in the absence and presence of cfMLP. A negative value for polarization results when more PH-Akt localizes to the dead end leading edge than to the open end leading edge. (*C*) Directional decision statistics of cells deciding after laser activation alone ("laser") or in the presence of cfMLP alone. (*D*) Column scatter dot plot of the maximum distance the dead-end side leading edge extended toward the dead end. Data are shown (left to right) for cells in the presence of cfMLP and laser excitation, the absence of both cfMLP and laser excitation, the presence of only cfMLP, and the presence of only laser excitation. (*E*) Column scatter dot plot of extension velocity of open end leading edge for cells that were exposed to cfMLP and laser excitation (purple) and laser excitation only (cyan), both directly before laser excitation and ∼18 s following laser excitation.
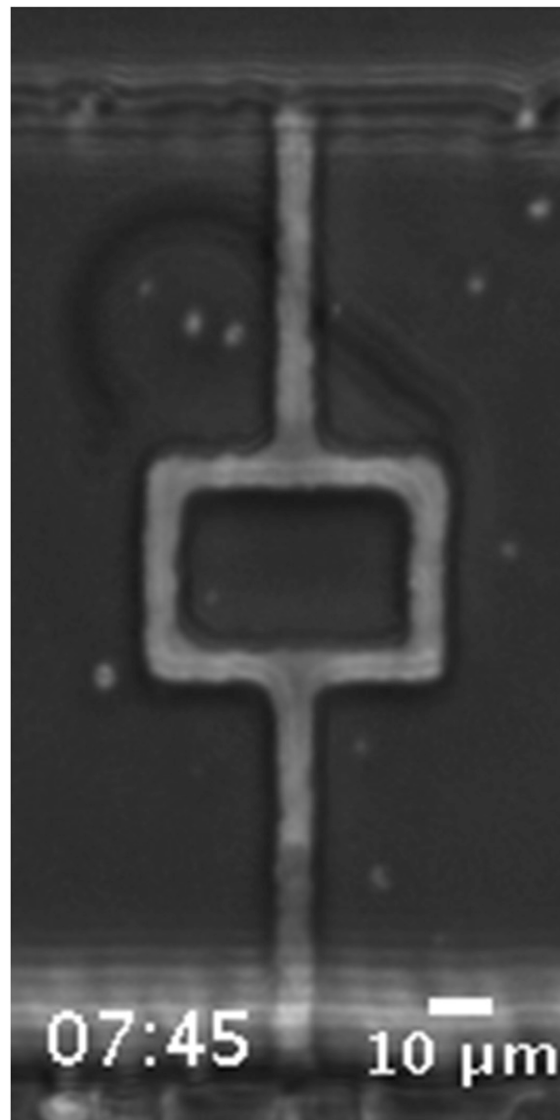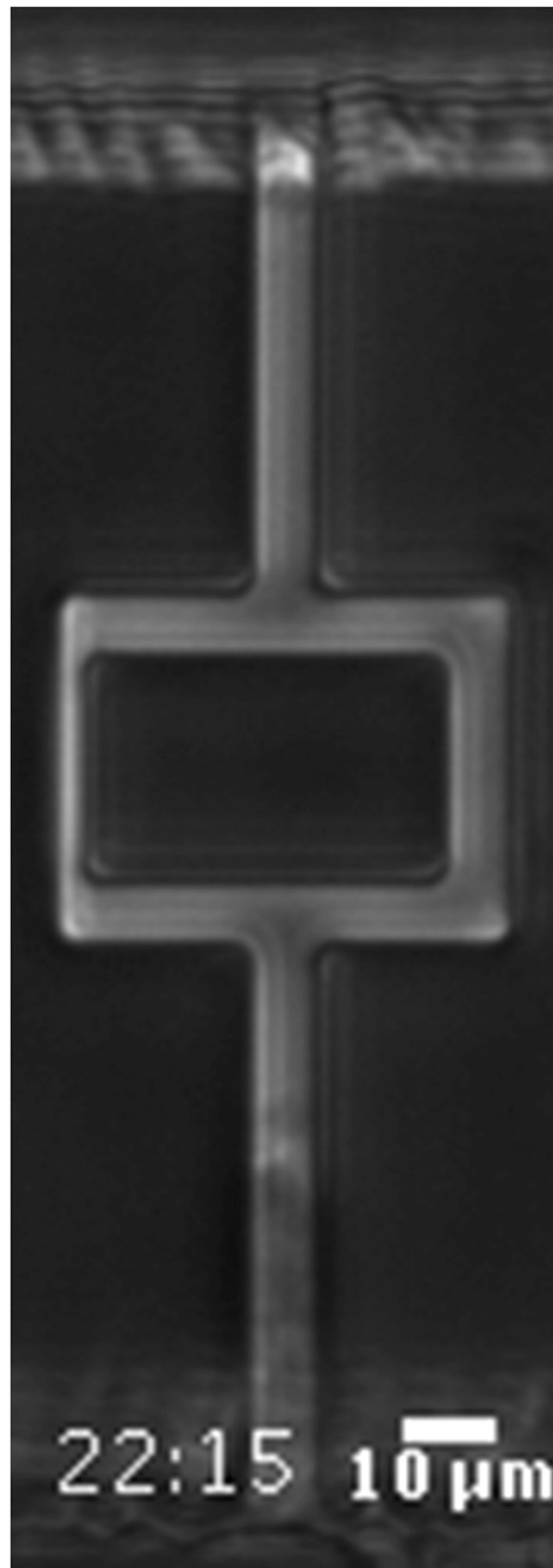
Movie S1. Video corresponding to montage in Fig. 1C of a cell migrating in a symmetrical bifurcating microchannel.
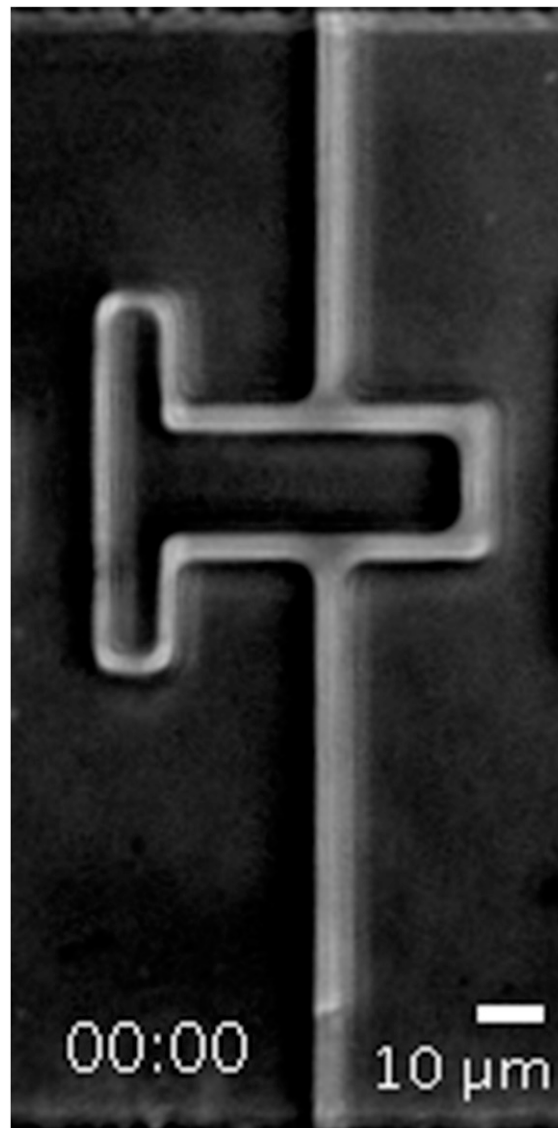
Movie S1
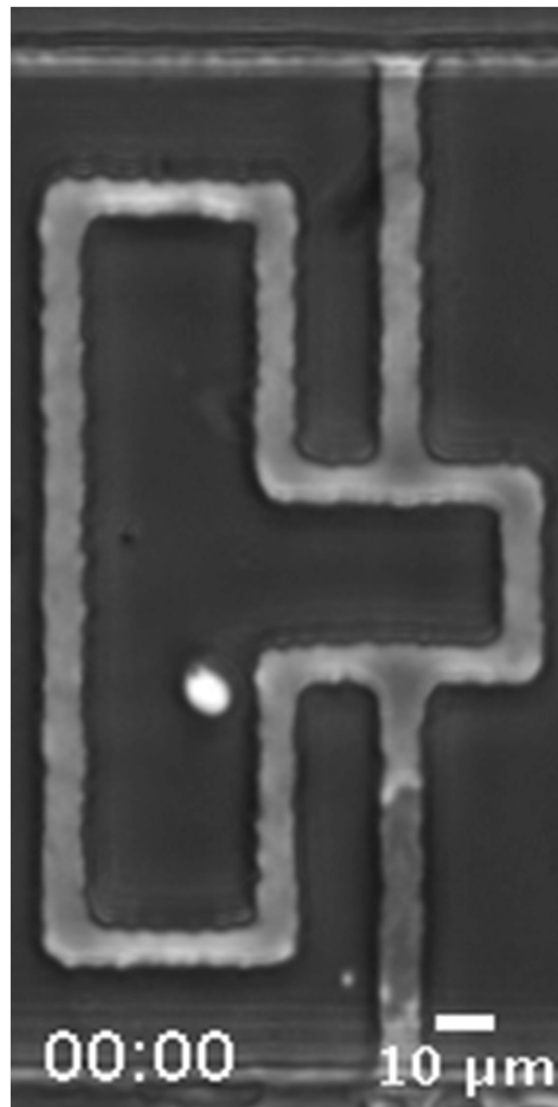
Movie S2. Video corresponding to montage in Fig. 1*D* of a cell migrating in an asymmetrical bifurcating microchannel.
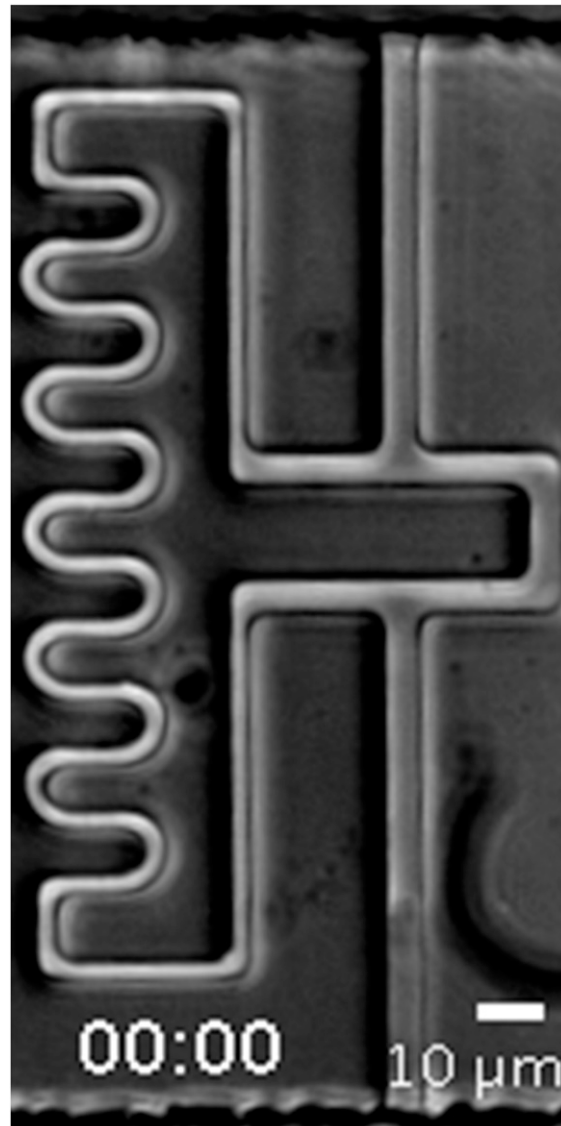
Movie S2

Movie S3. Video corresponding to montage in Fig. 2C of a cell migrating in the 4× resistance ratio bifurcating microchannel.
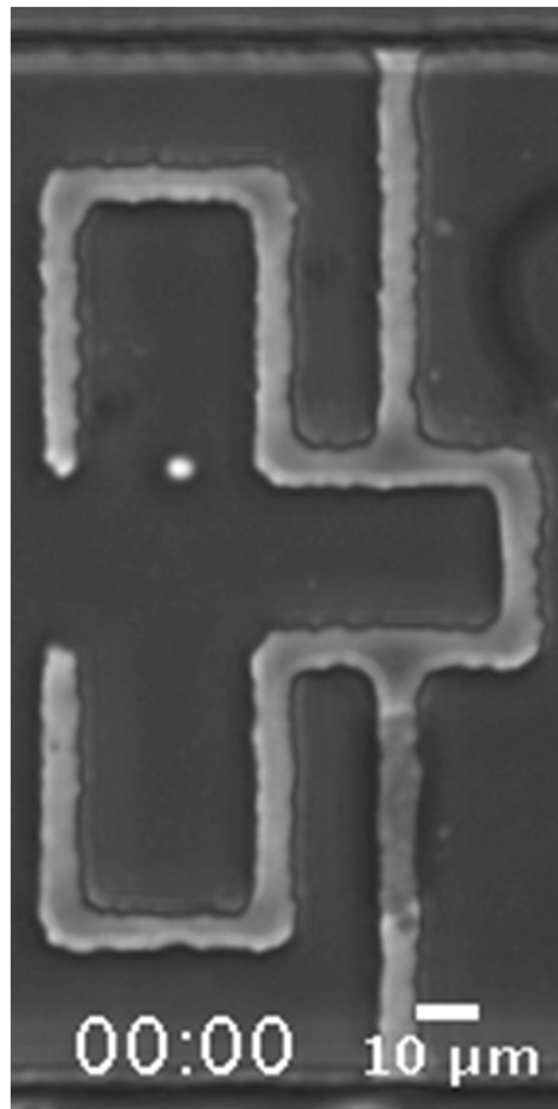
Movie S3

Movie S4. Video corresponding to montage in Fig. 2D of a cell migrating in an 8× resistance ratio asymmetrical bifurcating microchannel.
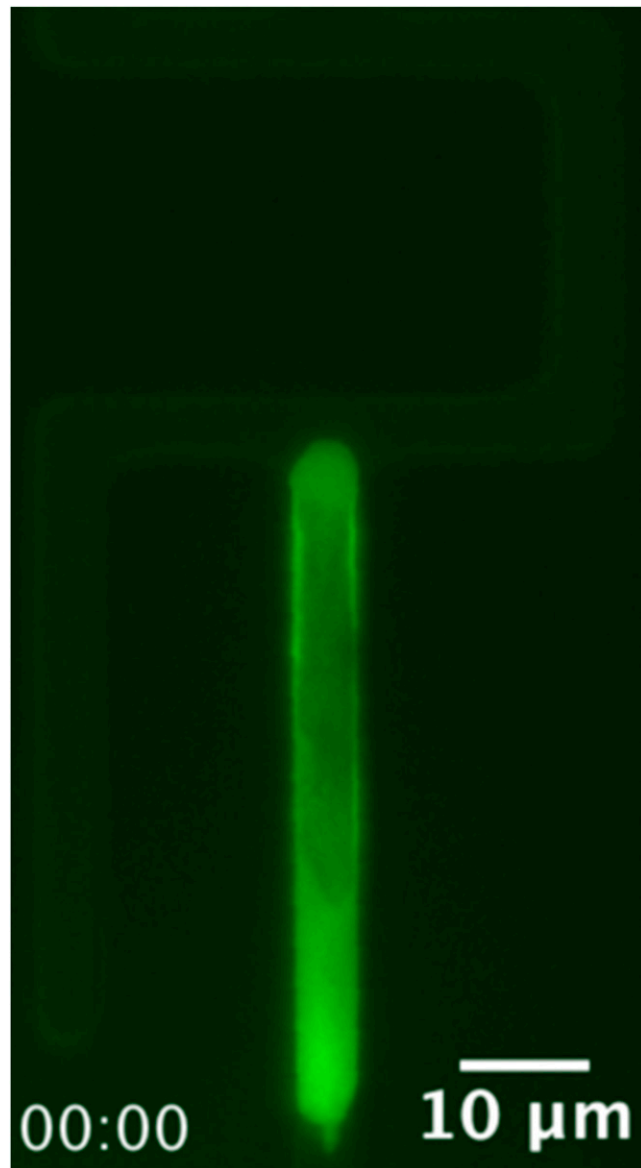
Movie S4

Movie S5. Video corresponding to montage in Fig. 2*E* of a cell migrating in an 32× resistance ratio asymmetrical bifurcating microchannel.
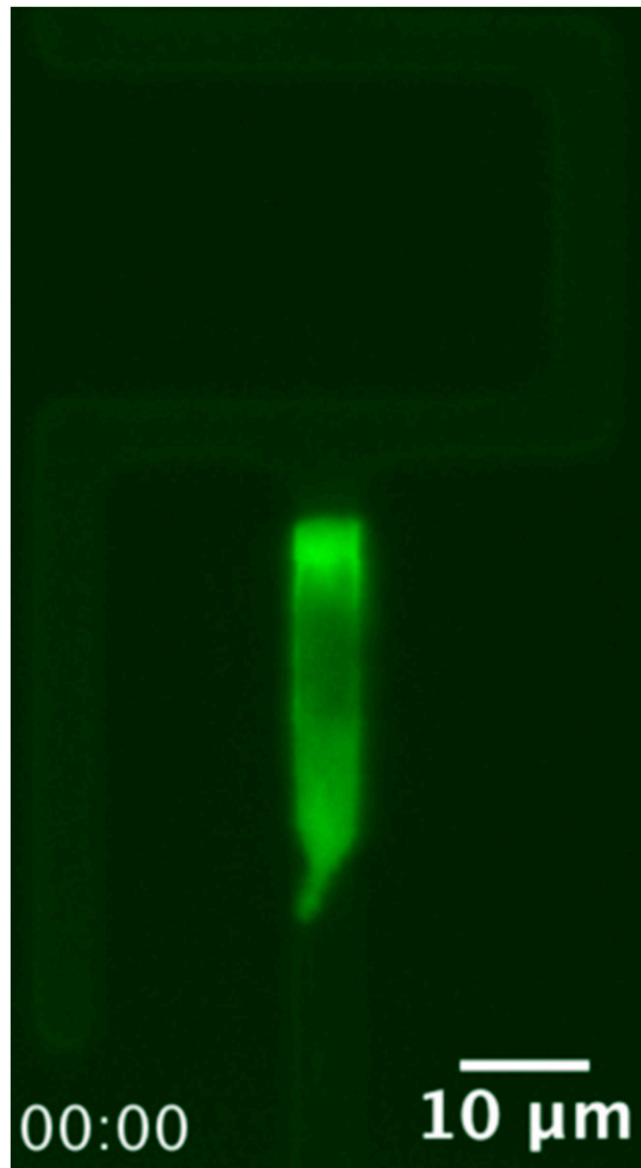
Movie S5

Movie S6. Video corresponding to montage in Fig. 2*F* of a cell migrating in a bifurcating microchannel with a dead-end branch.

Movie S6

Movie S7. Video corresponding to montage in Fig. 3*A* of a cell expressing the leading edge marker PH-Akt in a wide (6 μm width) asymmetrical bifurcating microchannel.

[Movie S7](#)

Movie S8. Video corresponding to montage in Fig. 3*B* of a cell expressing the leading edge marker PH-Akt in a narrow (3 μm width) asymmetrical bifurcating microchannel.

[Movie S8](#)

Movie S9.   Video corresponding to montage in Fig. 4*A* of a cell expressing the leading edge marker PH-Akt in a dead-end channel responding to uncaging of cfMLP and migrating down the open-end channel. White dot appears in frame following uncaging to mark location of laser excitation.

[Movie S9](#)

Movie S10. Video corresponding to montage in Fig. 4*B* of a cell expressing the leading edge marker PH-Akt in a dead-end channel responding to uncaging of cfMLP and migrating down the dead-end channel. White dot appears in frame following uncaging to mark location of laser excitation.

Movie S10